4-2014

Modeling the Thermosphere as a Driven-dissipative Thermodynamic System

William R. Frey

C. S. Lin

Matthew B. Garvin

Ariel O. Acebal
Air Force Institute of Technology

Recommended Citation

Frey, W. R., Lin, C. S., Garvin, M. B., & Acebal, A. O. (2014). Modeling the thermosphere as a driven-dissipative thermodynamic system. Space Weather, 12(3), 132–142. https://doi.org/10.1002/2013SW001014

AGU PUBLICATIONS

Space Weather

RESEARCH ARTICLE
10.1002/2013SW001014

Modeling the thermosphere as a driven-dissipative thermodynamic system

W. R. Frey[1,2], C. S. Lin[3], M. B. Garvin[2], and A. O. Acebal[2]

[1]Air Force Weather Agency, Offutt Air Force Base, Bellevue, Nebraska, USA, [2]Department of Engineering Physics, Air Force Institute of Technology, Wright-Patterson Air Force Base, Dayton, Ohio, USA, [3]Space Vehicles Directorate, Air Force Research Laboratory, Kirtland Air Force Base, Albuquerque, New Mexico, USA

Key Points:
- Thermospheric temperatures are modeled with solar UV and solar wind inputs
- Modified model produces lower temperature errors than that of Burke, 2011
- Model parameters are determined as functions of the F10.7 solar UV proxy

Correspondence to:
W. R. Frey,
billfrey35@gmail.com

Citation:
Frey, W. R., C. S. Lin, M. B. Garvin, and A. O. Acebal (2014), Modeling the thermosphere as a driven-dissipative thermodynamic system, *Space Weather*, *12*, 132–142, doi:10.1002/2013SW001014.

Received 13 NOV 2013
Accepted 17 FEB 2014
Accepted article online 18 FEB 2014
Published online 7 MAR 2014

Abstract Thermospheric density impacts satellite position and lifetime through atmospheric drag. More accurate specification of thermospheric temperature, a key input to current models such as the High Accuracy Satellite Drag Model, can decrease model density errors. This paper improves the model of Burke et al. (2009) to model thermospheric temperatures using the magnetospheric convective electric field as a driver. In better alignment with Air Force satellite tracking operations, we model the arithmetic mean temperature, $T_{1/2}$, defined by the Jacchia (1977) model as the mean of the daytime maximum and nighttime minimum exospheric temperatures occurring in opposite hemispheres at a given time, instead of the exospheric temperature used by Burke et al. (2009). Two methods of treating the solar ultraviolet (UV) contribution to $T_{1/2}$ are tested. Two model parameters, the coupling and relaxation constants, are optimized for 38 storms from 2002 to 2008. Observed $T_{1/2}$ values are derived from densities and heights measured by the Gravity Recovery and Climate Experiment satellite. The coupling and relaxation constants were found to vary over the solar cycle and are fit as functions of $F_{10.7a}$, the 162 day average of the $F_{10.7}$ index. Model results show that allowing temporal UV variation decreased model $T_{1/2}$ errors for storms with decreasing UV over the storm period but increased $T_{1/2}$ errors for storms with increasing UV. Model accuracy was found to be improved by separating storms by type (coronal mass ejection or co-rotating interaction region). The model parameter fits established will be useful for improving satellite drag forecasts.

1. Introduction

The thermosphere is defined as the neutral part of the Earth's upper atmosphere from roughly 95 to 1000 km above sea level. Hundreds of low-Earth orbit satellites operate at these altitudes. The ability to predict satellite position depends on accurate thermospheric density characterization [*Marcos et al.*, 2006]. Since thermospheric temperature is used as a parameter in existing models to determine densities [*Wise et al.*, 2012], a more accurate specification of temperature can be used to improve density forecasts. As the thermosphere becomes more crowded with low-Earth orbit satellites and space debris the potential consequences of inaccurate forecasts are becoming more significant. Recent events illustrate these consequences. The risk posed to operational satellites by space debris was illustrated in 2009 when the Iridium 33 satellite was destroyed by a collision with the non-operational Cosmos 2251 satellite [*Burke et al.*, 2010]. There have been several instances where the risk of collision with debris has forced the crew of the International Space Station to take emergency actions to ensure their safety [*Weimer et al.*, 2011]. Improved characterization of the thermospheric environment is necessary to increase space object tracking accuracy and allow satellite operators and manned spaceflight missions to anticipate and avoid collisions [*Wright*, 2007].

Variations in thermospheric density impact satellite orbit trajectories through variations in drag. The acceleration due to atmospheric drag is given by

$$a_{\text{drag}} = C_{\text{D}}\left(\frac{A_{\text{sc}}}{M_{\text{sc}}}\right)\rho V^2 \tag{1}$$

where A_{SC} and M_{SC} are the cross-sectional area and mass of the spacecraft, respectively, ρ is the neutral mass density of the atmosphere, and V is the spacecraft velocity relative to the neutral atmosphere. The drag coefficient C_{D} depends on the angle of flow to the spacecraft surface, the ratio of the temperatures of the spacecraft surface and the local atmosphere, and the ratio of the mean mass of atoms in the atmosphere to those on the spacecraft surface [*Cook*, 1965].

Accurate and continuous observations of thermospheric density have become readily available since 2002 from the Gravity Recovery and Climate Experiment (GRACE) [*Tapley et al*., 2004] satellite. Densities are derived from an on-board accelerometer that measures the electrostatic force needed to maintain a proof mass at the center of a cage located within 2 mm of the spacecraft's center of mass. Since the spacecraft and the proof mass respond to gravity in the same way, the changes in the electrostatic force needed to maintain the proof mass position reflect the spacecraft's response to non-gravitational forces such as thermospheric drag [*Bruinsma and Biancale*, 2003]. The availability of reliable in situ thermospheric density measurements allows relevant comparisons with current modeled densities as well as "ground truth" data with which to test new methods of modeling the thermospheric environment.

Changes in neutral density are driven by changes to the energy input to the thermosphere. The main energy inputs to the thermosphere are solar radiation in the EUV portion of the spectrum and energy transferred from the solar wind to the thermosphere through the magnetosphere in the forms of Joule heating and particle precipitation [*Knipp et al*., 2004]. Empirical thermospheric models such as MSIS (Mass Spectrometer and Incoherent Scatter Radar) [*Picone et al*., 2002], DTM (drag temperature model) [*Bruinsma et al*., 2012], and Jacchia [*Jacchia*, 1977] have generally tried to capture these inputs using combinations of solar proxies, such as the $F_{10.7}$ index, and geomagnetic indices such as the Ap index. The High Accuracy Satellite Drag Model (HASDM) [*Storz et al*., 2005] uses the $E_{10.7}$ index from the SOLAR2000 model [*Tobiska et al*., 2000] to account for solar EUV radiation while ingesting observed drag data from a set of calibration satellites to create spatially varying density corrections in near real time. More recently the Jacchia-Bowman 2008 (JB2008) model [*Bowman et al*., 2008] has improved on this empirical approach by including satellite observations of UV radiation and switching to the disturbance storm time (Dst) index to quantify energy input during storm conditions.

While the performance of empirical density models has improved during geomagnetic quiet conditions, errors during geomagnetic storming conditions have remained stubbornly high: up to 30% higher than during quiet time [*Marcos et al*., 2010]. During geomagnetic storms energy input to the thermosphere from the magnetosphere, specifically via Joule heating, can become dominant over EUV radiation [*Knipp et al*., 2004; *Wilson et al*., 2006; *Fuller-Rowell and Solomon*, 2010]. The geomagnetic indices used by empirical models do not fully capture the magnitude or temporal variation of this energy input [*Moe and Moe*, 2011] which contributes to the increase in errors during storm time. *Knipp et al*. [2013] showed this specifically for a set of storms in 2004 and 2005 where the Dst index did not properly describe the rapid changes occurring in the thermosphere during storm time.

Recent work has moved away from using geomagnetic indices in an effort to improve model performance, especially during storm time. *Choury et al*. [2013] used artificial neural networks (ANN) to predict exospheric temperatures that were fed back into DTM to improve density predictions. Others have focused on more directly quantifying energy input from the magnetosphere by using solar wind data. *Fedrizzi et al*. [2012] used the CTIPe (coupled thermosphere-ionosphere-plasmasphere electrodynamics) model [*Millward et al*., 2001] driven by solar wind data to generate Joule heating rates. The CTIPe Joule heating was compared to observed thermospheric densities to create a Joule heating index that was shown to improve empirical model neutral density forecasts. *Burke* [2007] showed that the cross polar cap potential is well correlated with density during storm time. *Liu et al*. [2010] used solar wind data to calculate the magnitude of the merging electric field, a quantity closely correlated to the polar cap potential defined as the electric field present in the region of the magnetosphere's tail where magnetic reconnection takes place. This was used along with the $F_{10.7}$ index in a linear equation to generate storm time densities. The results were shown to match storm time density changes observed by the CHAMP (Challenging Minisatellite Payload) satellite [*Bruinsma et al*., 2004]. *Weimer et al*. [2011] used the W05 model [*Weimer*, 2005] and interplanetary magnetic field (IMF) data to calculate corrections to the global nighttime minimum exospheric temperature, ΔT_c, which is done in JB2008 using the Dst index. Analysis showed that computing ΔT_c using IMF data instead of Dst produced an improved correlation with observations and could be used in JB2008 to improve accuracy.

This paper builds on the work of *Burke et al*. [2009] who used neutral density observations from the GRACE satellite along with the *Jacchia* [1977] (J77) model [*Jacchia*, 1977] to calculate the total energy content of the thermosphere, E_{th}, as the sum of the thermal and gravitational potential energy. The

magnitude of the dawn-to-dusk convective electric field in the inner magnetosphere, ε_{VS}, was modeled using observed solar wind data. According to *Burke* [2007], ε_{VS} may be represented as $\Phi_{PC}/2R_EL_Y$, where Φ_{PC} is the cross polar cap potential, R_E is Earth's radius, and L_Y refers to the equatorial distance from Earth's center to the magnetopause along the dawn or dusk meridian in units of R_E. See *Burke et al*. [2009] for details of computing ε_{VS}. *Burke et al*. [2009] show that E_{th} decays to pre-disturbance levels when ε_{VS} drops to pre-disturbance levels and the rate of decay, at least for two cases, was the same. The *e*-fold relaxation time of E_{th}, τ, was calculated to be 6.5 h. This behavior matches that of a driven-dissipative system. *Burke et al*. [2009] applied a driven-dissipative approach to model E_{th} using ε_{VS} as the driver. Since E_{th} is closely related to the orbit averaged exospheric temperature (T_∞), T_∞ can also be modeled in this way.

Burke et al. [2009] treated T_∞ as the result of two independent energy contributions, UV irradiance and the solar wind. During storm time the UV contribution was considered constant (850 K), and the rate of change in the orbit-averaged T_∞ was modeled using a differential equation.

$$\frac{dT_{\infty\,SW}}{dt} = \alpha\varepsilon_{VS} - \frac{T_{\infty\,SW}}{\tau} \tag{2}$$

In equation (2) $T_{\infty SW}$ is the solar wind contribution to T_∞, α is an empirical coupling constant accounting for coupling of the energy input from the solar wind through the magnetosphere, and τ is the empirical relaxation constant, taken to be 6.5 h. By solving equation (2) numerically with the Euler method and comparing results with GRACE data, *Burke et al*. [2009] obtained a value for the coupling constant. This model produced exospheric temperature values that agreed well with GRACE data. *Burke* [2011] analyzed a larger sample of storm periods and determined a unique coupling constant value for each storm period while keeping the relaxation constant fixed at 6.5 h. The value of the coupling constant was found to vary over the solar cycle and was fit well as a function of $F_{10.7a}$, the 162 day average of the daily $F_{10.7}$ index.

We built on the pioneering work of *Burke et al*. [2009] to model thermospheric temperatures using solar EUV irradiance and the magnetospheric electric field as drivers. By extending Burke's approach, a more rigorous test of the applicability of the driven-dissipative system model is obtained resulting in a more accurate, generalized model of thermospheric temperature. The remainder of this paper is structured as follows. Section 2 details the methodology used to develop the model formulation of this study, and section 3 presents the results of the updated model. Section 4 contains a discussion of main findings, compares the results with earlier work, and validates the model by applying it to test storms outside the original sample. Finally, section 5 presents a summary.

2. Methodology

2.1. The *Jacchia* [1977] Model

Because the J77 model [*Jacchia*, 1977] is an important part of this study a brief overview of its relevant features is provided here. J77 is a static empirical model developed using thermospheric densities inferred from satellite drag and mass spectrometer measurements. The mesopause is assumed to be at an altitude of 90 km with a temperature of 188 K and a mass density of 3.43 g*cm^{-3}. Model temperatures rise as a function of altitude from a minimum value at 90 km passing through an inflection point at 125 km and increasing asymptotically to a given exospheric temperature, T_∞. T_∞ uniquely defines the temperature profile. Once the temperature profile is determined, densities are calculated by integrating the thermal diffusion equation

$$\frac{dn_i}{n_i} = -\frac{m_i g}{R^* T}dz - \frac{dT}{T}(1 + a_i) \tag{3}$$

where the index *i* denotes the i^{th} species, *n* is the number density, *m* is the mass, *g* is gravity, *a* is the thermal diffusion coefficient, *T* is the temperature, and R^* is the universal gas constant. The J77 model includes six species: N_2, O_2, O, Ar, He, and H. The total mass density at a given altitude can be calculated by simply summing the product $n_i m_i$ over all species [*Wise et al*., 2012]. Through this process, tables are produced that give density profiles for a given exospheric temperature input.

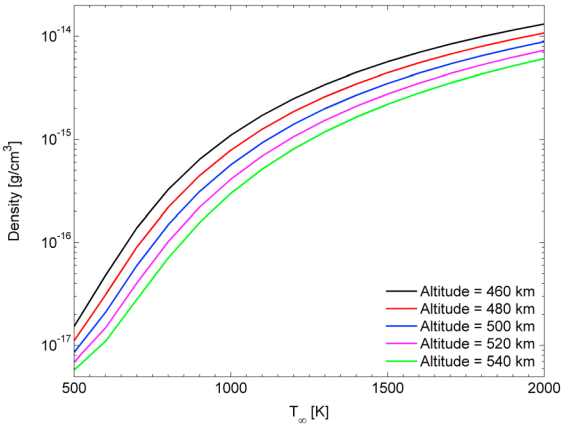

Figure 1. Neutral density computed using the J77 model [*Jacchia*, 1977] is plotted vs exospheric temperature (T_∞) for altitudes representative of the Gravity Recovery and Climate Experiment (GRACE) satellite's location from 2002 to 2008.

T_∞ is a local parameter and at a given instant the global distribution of T_∞ includes a nighttime minimum, T_0, and a daytime maximum, T_M, in opposite hemispheres. The arithmetic mean of T_0 and T_M is referred to as the arithmetic mean temperature, $T_{1/2}$. If $T_{1/2}$ is known, the local T_∞ can be computed for any location on the globe using the relationship

$$T_{1/2} = \frac{T_\infty}{D(\delta, \varphi, H)} \tag{4}$$

The conversion factor D is a function of solar declination angle (δ), latitude (φ), and solar hour angle (H) and given by

$$D = 1 + c_1 \frac{\delta}{\varepsilon} \sin(\phi) + c_2 \left(f(H) - \frac{1}{2} \right) \cos(\phi) \tag{5}$$

where:

$$f(H) = \cos^3 \left[\frac{1}{2}(H + \beta) \right] + c_3 \cos[3(H + \beta) + \chi]$$

$$c_1 = 0.15, c_2 = 0.24,\ c_3 = 0.08, \beta = -60^o,\ \varepsilon = 23.44^o,\ \chi = -75^o$$

The hour angle H is simply local standard time converted to an angle counted from local noon via the formula:

$$H = (\text{local time (h)} - 12) \times 15^o \tag{6}$$

It is important to emphasize that $T_{1/2}$ describes the arithmetic mean of T_0 and T_M at a given instant and not the mean of the diurnal extremes in a given location's T_∞ over a 24 h period. $T_{1/2}$ varies on time scales shorter than 24 h, for example it could vary over the roughly 90 min time period of a GRACE orbit and can be used to determine the global distribution of T_∞ at any given time. The global nature of $T_{1/2}$ is useful as it allows energy inputs to the thermosphere to be accounted for by calculating their impact on $T_{1/2}$.

2.2. Data Description

Burke [2011] used hourly solar wind data during a sample of 38 geomagnetic storm periods from 2002 to 2008 to test his model. The present study uses 1-min solar wind data to improve accuracy. Because 1-min cadence solar wind data were not available for one event (Julian Date (JD) 168 to 170, 2003) used by *Burke* [2011] this storm was replaced by one from JD 94 to 98, 2004. Outside this one exception, the same storms considered by *Burke* [2011] are considered here.

Data from the GRACE A satellite [*Sutton*, 2011] were used to derive the "observed" exospheric temperature, T_∞. Tables of data from the J77 [*Jacchia*, 1977] model were generated using the formulation of D. L. Huestis [*Jacchia*, 1977 Atmospheric Model, 2002, http://nssdcftp.gsfc.nasa.gov/models/atmospheric/jacchia/jacchia-77/j77sri.for]. The output tables list densities as a function of altitude from 300 to 1000 km with a resolution of 1 km for a given exospheric temperature. Within J77 density increases as a function of exospheric temperature rather smoothly at GRACE altitudes as shown in Figure 1. Therefore, to save computation time tables were generated with a temperature resolution of 100 K for exospheric temperatures from 500 to 2000 K. The J77 tables were used to create a 3-D data grid giving density for a specified T_∞, altitude pair. The temperature and altitude ranges chosen ensure that all of the observed GRACE data fit inside the data grid. With the grid as a basis, a density can be generated using any specified T_∞, altitude pair by interpolating between the data points. To generate exospheric temperatures from observed GRACE heights and densities an iterative technique, the Nelder-Mead simplex direct-search method [*Lagarias et al.*, 1998], was used. Starting at an initial guess for T_∞, here 800 K, the search method iterates over T_∞ values until a T_∞ is found that minimizes the relative error (to a tolerance of 10^{-4}%) between the observed density and the interpolated density when paired with the observed altitude. Note that the temperature calculated here from GRACE data is not a physical temperature

but a model temperature only consistent with the J77 model. To follow more closely with current Air Force satellite tracking operations, T_∞ values were converted to $T_{1/2}$ via equation (4). The GRACE-derived $T_{1/2}$ data were then orbit averaged. Orbit-averaged $T_{1/2}$ values were used as the observed data the model attempts to replicate.

2.3. Energy Inputs

The most variable source of energy for the thermosphere during geomagnetic storms is the solar wind which couples to the thermosphere via the magnetospheric electric field, ε_{VS}. Using solar wind data from the Advanced Composition Explorer (ACE) satellite, ε_{VS} can be calculated in near real time using a version of the Volland-Stern model originally formulated by *Ejiri* [1978] and modified by *Burke* [2007]. This same procedure was used in previous work [*Burke et al*., 2009; *Burke*, 2011; *Frey*, 2013]. ACE data were used to calculate ε_{VS} at each minute during the storm periods. Interpolation was used to bridge short gaps in ACE data.

To account for the UV contribution to thermospheric temperatures the method of the J77 model was used where the UV contribution to $T_{1/2}$ ($T_{1/2UV}$) is calculated via the formula

$$T_{1/2UV}(t) = 5.48(F_{10.7a})^{0.8} + 101.8(F_{10.7})^{0.4} \tag{7}$$

where $F_{10.7}$ is the daily value of the $F_{10.7}$ index and $F_{10.7a}$ is its 162 day averaged value.

2.4. Governing Equation

The time rate of change in $T_{1/2}$ can be expressed as the sum of UV and solar wind contributions.

$$\frac{dT_{1/2}}{dt} = \frac{dT_{1/2UV}}{dt} + \frac{dT_{1/2SW}}{dt} \tag{8}$$

Just prior to storm time the thermosphere is taken to be at equilibrium with the time rate of change in $T_{1/2}$ equal to zero and

$$T_{1/2} = T^0_{1/2} = T^0_{1/2UV} + T^0_{1/2SW} \tag{9}$$

Equation (9) expresses the pre-storm equilibrium arithmetic mean temperature ($T^0_{1/2}$) as the sum of the equilibrium UV and solar wind contributions. Outside geomagnetic storming periods the UV contribution to thermospheric energy is much larger than the solar wind contribution [*Knipp et al*., 2004] which indicates that $T^0_{1/2UV} >> T^0_{1/2SW}$, suggesting the approximation $T^0_{1/2} \approx T^0_{1/2UV}$.

Using equation (2) for the time rate of change of the solar wind contribution to $T_{1/2}$ and substituting $T_{1/2SW} = T_{1/2} - T_{1/2UV}$, equation (8) becomes:

$$\frac{dT_{1/2}}{dt} = \frac{dT_{1/2UV}}{dt} + \alpha\varepsilon_{VS}(t) - \frac{T_{1/2}(t) - T_{1/2UV}(t)}{\tau} \tag{10}$$

Solving equation (10) using Euler's method provides a model of $T_{1/2}$ as a function of time.

$$T_{1/2}(t + \Delta t) = T_{1/2}(t) + \Delta t\left[\frac{dT_{1/2UV}}{dt}(t) + \alpha\varepsilon_{VS}(t) - \frac{T_{1/2}(t) - T_{1/2UV}(t)}{\tau}\right] \tag{11}$$

A time step (Δt) of 1 min was used to match the cadence of the ACE-derived magnetospheric electric field data. Equation (11) shows that any solution for $T_{1/2}$ depends on the way in which $T_{1/2UV}$ is treated. Two different methods were tested in this study.

Method One: The simplest way to treat $T_{1/2UV}$ is to approximate it as the constant $T^0_{1/2}$ through the storm period and thus $dT_{1/2UV}/dt = 0$. This is the method *Burke et al*. [2009] used in their original model. In method one, $T^0_{1/2}$ was defined as the mean of the observed arithmetic mean exospheric temperature from the eight GRACE orbits (≈12 h) prior to the storm start time.

Method Two: Both $T_{1/2UV}$ (t) and $dT_{1/2UV}/dt$ are considered to be time dependent.

To obtain values for $T_{1/2UV}(t)$, equation (7) was used to calculate a value for $T_{1/2UV}$ at 20 Coordinated Universal Time each day and then interpolated to produce a value at each minute. Because $T_{1/2UV}$ as defined in equation (7) is a modeled input, it does not always match the observed value of $T^0_{1/2}$, as defined in method

Table 1. Model Statistics

	Mean α	Std Dev α	Mean τ	Std Dev τ	Mean Error	Std Dev Error
Method 1	35.03	13.90	7.71	3.07	2.04%	0.94%
Method 2	34.65	12.87	8.25	3.05	1.84%	0.80%
[*Burke*, 2011]	36.07	17.00	6.50	0.00	3.62%	2.26%

one, at the beginning of the storm period. To remove this discrepancy a correction factor, equal to the difference between the observed value of $T_{1/2}$ and the modeled value of $T_{1/2UV}$ at the start the storm, was added to the modeled value of $T_{1/2UV}$ at each time. Using the results of equation (7), the time rate of change of $T_{1/2UV}$ was calculated for each minute during the storm period as:

$$\frac{dT_{1/2UV}}{dt}(t) = \frac{T_{1/2UV}(\text{next observation}) - T_{1/2UV}(\text{prior observation})}{24\,\text{h}} \tag{12}$$

Equation (12) results in a value for each minute during the storm period with units of K/h. The J77 formulation for $T_{1/2UV}$ in equation (7) results in values for its time rate of change that are constant, but not necessarily zero, for 24 h periods between $F_{10.7}$ observations.

After modeled $T_{1/2}$ values are calculated for each minute of the storm period the modeled values were orbit averaged over the same time periods defined earlier by the GRACE orbits. The values of both α and τ were considered constant through each storm period but were allowed to have different values for each storm period and for each method. To determine the optimal value of α and τ for each storm period, the Nelder-Mead simplex direct-search method [*Lagarias et al.*, 1998] was used to minimize the relative root-mean-square (RMS) error, defined by equation (13), between the observed and modeled values of $T_{1/2}$ by adjusting the values of α and τ.

$$\text{Relative } T_{1/2}\,\text{RMS error} = \sqrt{\frac{1}{N}\sum \frac{\left(T_{1/2}^{\text{Observed}} - T_{1/2}^{\text{Model}}\right)^2}{\left(T_{1/2}^{\text{Observed}}\right)^2}} \tag{13}$$

Here $T_{1/2}{}^{\text{Observed}}$ denotes the orbit-averaged observed $T_{1/2}$ values derived from GRACE data, $T_{1/2}{}^{\text{Model}}$ denotes the orbit-averaged model $T_{1/2}$ values using one of the methods described above, and N is the number of data points, or orbits, during the storm period.

To summarize the methodology, this study builds on the approach of *Burke et al.* [2009] in the following areas:

1. We have modeled $T_{1/2}$ in this study in place of T_{∞}.
2. Energy input to the thermosphere from solar extreme ultraviolet (EUV) irradiance is allowed to vary through each storm period.
3. A rigorous approach is applied to determine the optimal values for both the coupling and relaxation constants.

3. Result

Table 1 lists the mean and standard deviation of α, τ, and the relative $T_{1/2}$ RMS error for methods one and two. Method two has mean α values lower than method one and mean τ values slightly higher. The mean relative RMS error for method two is 10% less than that of method one. Table 1 also shows results produced using the model of *Burke* [2011]. The results from *Burke* [2011] were produced using the α values listed by *Burke* [2011] for each storm and a constant τ of 6.5 h. Both method one and method two produce mean relative RMS errors lower than those from the model of *Burke* [2011].

Coupling constant (α) values range from roughly 17 to 68 (K/h)/(mV/m) for methods one and two with values most frequently falling between 20 and 30 (K/h)/(mV/m). Higher α values amplify the impact of ε_{VS} on $T_{1/2}$ in the model due to the term $\alpha\varepsilon_{VS}(t)$ in equation (10). Therefore, storms with larger temperature rises will require higher α values. The α values for method two are slightly more closely spaced than those of method one as evidenced by the slightly smaller standard deviation of 12.87 (K/h)/(mV/m) for method two vs. 13.90 (K/h)/(mV/m) for method one.

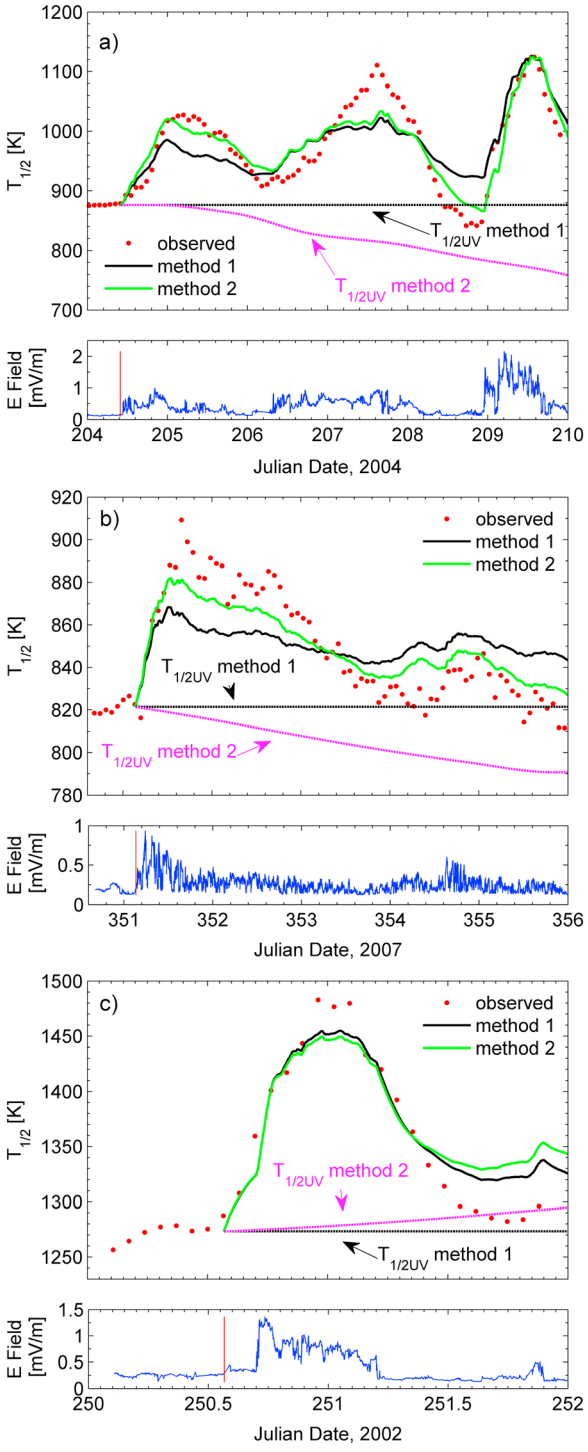

Figure 2. Model results for (a) the coronal mass ejection (CME) storm from Julian Date (JD) 204-210, 2004, (b) the CIR storm from JD 351-356, 2007, and (c) the CME storm from JD 250-252, 2002. For each storm, the top plot shows observed GRACE $T_{1/2}$ (red dots), along with model $T_{1/2}$ results for methods one (black) and two (green). The dotted black line shows the result of the approximation $T_{1/2UV}(t) \approx T^0_{1/2}$ used in method one, and the pink dotted line shows the $T_{1/2UV}(t)$ used for method two. The bottom plot for each storm shows the electric field values calculated from Advanced Composition Explorer (ACE) data as a function of time. The red vertical line indicates the storm starting time.

The relaxation constant controls how quickly $T_{1/2}$ recovers to near pre-storm levels after ε_{VS} returns to normal. Storms with a faster recovery result in lower τ values. Relaxation constant values ranged from roughly 3 to 15 h for both methods with values falling most frequently between 5 and 7.5 h. The range in τ values was significantly smaller than the range in α values indicating that the recovery period of geomagnetic storms is less variable than the main phase. The spread in τ values was similar for both methods, with standard deviations just over 3 h.

Figure 2 shows the $T_{1/2}$ results of the model for three storms out of the 38 storm sample. Both the JD 204-210, 2004 coronal mass ejection (CME)-driven storm (a) and the JD 350-356, 2007 co-rotating interaction region (CIR)-driven storm (b) have decreasing UV contributions over the storm periods. For both of these storms method two clearly outperformed method one. Allowing $T_{1/2UV}$ to decrease by definition increases $T_{1/2SW}$ which results in higher α values for method two. Decreasing $T_{1/2UV}$ also results in higher τ values for method two. During the relaxation period of a storm, decreasing $T_{1/2UV}$ lowers the temperature toward which the thermosphere recovers, resulting in longer relaxation times.

Method two produced larger errors than method one for nine storms in the sample. Figure 2c shows the results for one of these storms, the CME storm from JD 250 to 252, 2002. Unlike the two previous storms, here $T_{1/2UV}$ increases throughout the storm period. This causes τ for method two to be lower than method one, resulting in the decreased accuracy near the peak of the storm. In addition, method two models the recovery phase of the storm worse than method one because the increasing $T_{1/2UV}$ increases the method two modeled time rate of change of $T_{1/2}$ during a time when observed $T_{1/2}$ is decreasing.

Robinson and Vondrak [1984] showed that both the ion-electron production rate and ionospheric conductance are correlated with $(F_{10.7})^{1/2}$, leading *Burke* [2011] to suggest that the thermosphere's response to storm time energy inputs varies over the solar cycle. To test this α and τ values obtained with method two were fit as functions of $F_{10.7a}$. In Figure 3 all storm fits are shown in black, CME storm fits

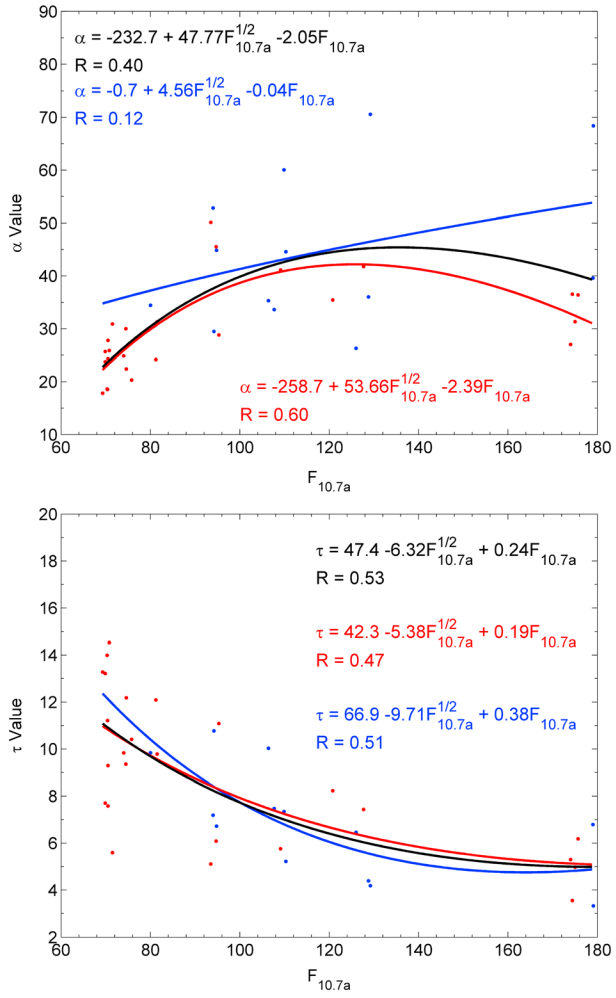

Figure 3. (Top) Coupling constant (α) and (bottom) relaxation constant (τ) as functions of $F_{10.7a}$. Best fits of α and τ as quadratic functions of $(F_{10.7a})^{1/2}$ are shown. CME storms are shown in blue, CIR storms in red. The black line shows the best fit applied to all storms.

are shown in blue, and CIR storm fits are shown in red for α (top) and τ (bottom). The quadratic fit of α to $(F_{10.7a})^{1/2}$ for all storms, shown in black, produces a correlation of $R = 0.40$. Fits for α as a quadratic function of $(F_{10.7a})^{1/2}$ are also shown for CME storms (blue) and CIR storms (red). The fit for α limited to CME storms exhibits a very low correlation, $R = 0.12$, and is nearly a straight line. CME storms generally had higher α values than CIR storms. In fact, all storms with $\alpha > 50$ (K/h)/(mV/m) are CMEs, while all of the storms with $\alpha < 25$ (K/h)/(mV/m) are CIR storms. CIR storms are fit much better as a function of $(F_{10.7a})^{1/2}$ with a correlation of $R = 0.60$, much improved from the all-storms fit. These results indicate that the thermosphere responds differently to energy inputs from CME and CIR-driven storms.

Figure 3 (bottom) shows τ as a function of $F_{10.7a}$ for all storms (black), CME storms (blue), and CIR storms (red) using method two data. Again, a quadratic least squares fit was constructed of τ as a function of $(F_{10.7a})^{1/2}$. The correlation of $R = 0.53$ for all storms is higher than the correlation for α. The best fit curves for both storm types are similar, with correlations of $R = 0.47$ and $R = 0.51$ for CIRs and CMEs, respectively. The correlations are worse for both storm types than the correlation of the all storms fit indicating that the relaxation times for different storm types depend similarly on $F_{10.7a}$. In general, τ values are higher for CIR storms. All storms with $\tau > 11$ h are CIR driven.

The model was run with method two procedures for all 38 storms using α and τ values determined via the quadratic equations shown in Figure 3. Table 2 shows the mean $T_{1/2}$ relative RMS errors, calculated using equation (12), that result from optimal α and τ values for each storm, along with relative RMS errors that result from the all storms fit, CME fit, and CIR fit α and τ values. Column 2, labeled All Storms Mean, shows that the mean $T_{1/2}$ RMS error increased from 1.84% to 3.15% for all 38 storms when using the all storms fit α and τ values. For CME and CIR storms errors increased over the optimal values, though not drastically, when both the all storms fit and the storm specific fit was applied. For both storm types, the storm type specific fit values of α and τ produced a lower average RMS error than the all storms fit. Applying best fit curves to determine α and τ for each storm also created more spread in the relative $T_{1/2}$ RMS error values. Table 2 shows standard

Table 2. Relative $T_{1/2}$ RMS Error Results Using Best Fit α and τ Values With Method Two

	All Storms		CME Storms		CIR Storms	
	Mean	Std Dev	Mean	Std Dev	Mean	Std Dev
Optimal α and τ	1.84%	0.80%	2.17%	0.83%	1.67%	0.75%
All storms fit α and τ	3.15%	1.68%	4.37%	2.00%	2.52%	1.06%
CME-fit α and τ			4.01%	1.77%		
CIR-fit α and τ					2.24%	1.01%

Table 3. Test Storm Data

				Optimal			All Storms Fit			Storm Type Fit		
Year	Start Day	End Day	Storm Type	α	τ	RMS (%)	α	τ	RMS (%)	α	τ	RMS (%)
2003	308	309	CME	39.01	4.46	0.98	45.54	6.47	2.89	46.42	5.50	2.17
2004	42	45	CIR	28.74	8.56	1.05	44.99	6.81	2.52	42.46	5.98	1.43

deviations of the relative RMS error for each of the different fits. In all cases, the standard deviation increased over the value for the optimal α and τ case.

4. Discussion

Burke [2011] determined α values for 37 of the 38 storms considered in this study. To compare *Burke*'s [2011] results with current results, the α values in *Burke* [2011] need to be divided by the J77 conversion factor given in equation (5) to account for the fact that he modeled T_∞ instead of $T_{1/2}$. The storm average conversion factor was generally near 0.95. The average value is simply obtained by calculating the conversion factor for each GRACE data point and then taking an average. The mean and standard deviation of the converted α values from *Burke* [2011] are shown in Table 1. Also, note that *Burke* [2011] has a mean error (3.62%) higher than our method one (2.04%) even though both assumed constant UV contribution to temperature. Both the α values and errors from *Burke* [2011] differ from those found in the present study. There are several reasons for the difference. First, *Burke* [2011] assumed that τ was constant over all storms. Allowing τ to change between storms impacts the value of α. In addition, *Burke* [2011] used 1-h averaged solar wind data to calculate ε_{VS} values and a time step of 1 h when applying equation (10) rather than the 1 min time step used here. Further, in this study the Nelder-Mead simplex direct-search method was applied in order to rigorously determine the best α and τ values. By running multiple versions of the model and isolating each procedural difference it was determined that the procedure to determine α and τ values for each storm has the biggest impact on the results and significantly decreases model errors.

The method that produced the lowest error for a given storm was dependent on the nature of the change (either increasing or decreasing) in $T_{1/2UV}$ over the storm period. Method two produced the lowest errors for 27 of the 28 storms with decreasing $T_{1/2UV}$, while method one produced the lowest errors for eight out of the ten storms with increasing $T_{1/2UV}$. This likely indicates that the effects of temporal $T_{1/2UV}$ variation have not yet been fully modeled.

The results of the model using best fit α and τ values, shown in Table 2, indicate that relatively low errors can be obtained using model parameters determined without prior knowledge of storm time $T_{1/2}$ values as would be required in a real-time modeling scenario. To test this conjecture the model with best fit α and τ values was applied to two storms, one CME and one CIR, outside the original sample. Due to the constraints of GRACE data availability, both test storms were within the same time frame of the original storms (2002 to 2008). Test storms were selected based on the availability of ACE data needed to calculate storm time ε_{VS} values.

Table 3 shows from left to right the year, start day, end day, and storm type for each test storm. Then α and τ values along with $T_{1/2}$ RMS errors are shown for the optimal case (minimum $T_{1/2}$ RMS error) as well as with the all storms and storm type specific best fits applied. For both test storms, the best fit values of α and τ produced reasonable results. For the JD 308 to 309, 2003 CME the relative $T_{1/2}$ RMS errors produced using the all storms fit and CME-fit α and τ values are more than double the optimal error, but they are also less than the best fit average errors for CME storms in the original sample (Table 2). Similarly, for the CIR test storm, the relative $T_{1/2}$ RMS errors produced using the all storms fit and the CIR fit α and τ values are also less than or equal to the average errors for CIR storms in the original sample with the CIR storm fit producing lower errors than the all storms fit. These results indicate that the best fit α and τ values are reasonable even outside the original sample and could be used without any prior knowledge of the geomagnetic storm to be modeled. We have used GRACE data for the test storms in order to allow for more direct comparisons with the earlier work of *Burke et al.* [2009] and *Burke* [2011]. In future work it will be useful to further validate these results using other satellite density data, for example CHAMP accelerometer data.

The errors produced by method two of the driven-dissipative model are of similar magnitude to published results of other recent models [*Choury et al.*, 2013; *Weimer et al.*, 2011]. The ANN model of *Choury et al.* [2013]

produced temperature errors of 1.6% and 1.31% for the years of 2004 and 2008, respectively, when compared to GRACE data. These errors include both periods of storming and quiet conditions. *Weimer et al*. [2011] reported average errors resulting from calculations using the W05 model of 0.97% to 3.28%.

The temperatures calculated in our paper are model temperatures consistent with the J77 model. The GRACE density derived from *Sutton* [2011] could potentially still have a small unknown bias even after careful removal of known satellite attitude biases (private communication with E. K. Sutton). In such a case $T_{1/2}$ deduced from the GRACE data would be affected by a scale factor γ due to density bias such that $T_{1/2} = \gamma\, T^{U}_{1/2}$, where is $T^{U}_{1/2}$ is the unbiased value. Substitution of this definition into equation (10) yields that the α value would be affected by a factor of $1/\gamma$ while the τ value remains unchanged.

The driven-dissipative model could be used currently in conjunction with observations from an upstream solar wind monitor such as the ACE satellite to produce temperature predictions with 30–60 min of lead time. After its launch in early 2015, the Deep Space Climate Observatory (DSCOVER) satellite will monitor solar wind velocity, density, and magnetic field conditions at the Sun-Earth L1 Lagrangian point. This will continue to provide a reliable source of solar wind data crucial for our model and other space weather forecasting applications into the future. With more development, the driven-dissipative approach could be integrated with solar wind models to provide forecasts with greater lead times and improve the accuracy of satellite drag models.

5. Summary

This paper has presented results from a driven-dissipative system model of thermospheric temperatures based on the work of *Burke et al*. [2009]. Several improvements were made to the model with the goal of increasing accuracy and investigating the impact of some of the simplifying assumptions made in the original formulation. The improved model produced lower mean $T_{1/2}$ RMS errors than the model developed previously by *Burke* [*Burke et al*., 2009; *Burke*, 2011]. It was demonstrated that the impact of UV temporal variation in the driven-dissipative model was significant. Allowing the time rate of change of $T_{1/2UV}$ to be nonzero decreases the mean RMS error for estimating thermospheric temperature when $T_{1/2UV}$ is decreasing. When $T_{1/2UV}$ increases over the storm period the model performs better by ignoring the $T_{1/2UV}$ temporal variation. This may imply that the effects of $T_{1/2UV}$ temporal variation have not yet been adequately modeled. Further study will need to remedy this deficiency. Values of the two empirical parameters in the driven-dissipative model, the solar wind-magnetosphere coupling constant and the thermospheric relaxation constant, exhibit solar cycle dependence and can be determined as functions of the $F_{10.7}$ solar irradiance proxy. This provides a convenient way to determine model parameters without any prior knowledge of a geomagnetic storm. Model accuracy was also found to be improved by separating storms by type (CME or CIR). The general applicability of the model and the model parameter fits established here will be useful to improve the density forecasts necessary to increase space object tracking accuracy in order to avoid spacecraft collisions.

Acknowledgments

W. Frey was sponsored by the Air Force Institute of Technology. W. Frey is currently the Air Force Weather Agency's Liaison Officer to the National Oceanic and Atmospheric Administration's Space Weather Prediction Center. The authors would like to thank E. K. Sutton for providing the GRACE neutral density data and NASA's OMNIWeb for the use of their ACE solar wind data. The views expressed in this article are those of the authors and do not necessarily reflect the official policy or position of the Air Force, the Department of Defense, or the U.S. Government.

References

Bowman, B. R., W. Tobiska, F. Marcos, C. Huang, C. Lin, and W. Burke (2008), A new empirical thermospheric density model JB2008 using new solar and geomagnetic indices, *AIAA/AAS Astrodynamics Specialist Conference, AIAA 2008-6438*.

Bruinsma, S., and R. Biancale (2003), Total densities derived from accelerometer data, *J. Spacecr. Rockets*, *40*, 230–236.

Bruinsma, S., D. Tamagnan, and R. Biancale (2004), Atmospheric densities derived from CHAMP/STAR accelerometer observations, *Planet. Space Sci.*, *52*, 297–312.

Bruinsma, S., N. Sánchez-Ortiz, E. Olmedo, and N. Guijarro (2012), Evaluation of the DTM-2009 thermosphere model for benchmarking purposes, *J. Space Weather Space Clim.*, *2*, doi:10.1051/swsc/2012005.

Burke, W. J. (2007), Penetration electric fields: A Volland-Stern approach, *J. Atmos. Sol. Terr. Phys.*, *69*, 1114–1126, doi:10.1016/j.jastp.2006.05.027.

Burke, W. J. (2011), Solar Cycle Dependence of Solar Wind Energy Coupling to The Thermosphere, *J. Geophys. Res.*, *116*, A06302, doi:10.1029/2011JA016437.

Burke, W. J., C. S. Lin, M. P. Hagan, C. Y. Huang, D. R. Weimer, J. O. Wise, L. C. Gentile, and F. A. Marcos (2009), Storm time global thermosphere: A driven-dissipative thermodynamic system, *J. Geophys. Res.*, *114*, A06306, doi:10.1029/2008JA013848.

Burke, W. J., L. C. Gentile, and M. P. Hagan (2010), Thermospheric Heating by High-Speed Streams in the Solar Wind, *J. Geophys. Res.*, *115*, A06318, doi:10.1029/2009JA014585.

Choury, A., S. Bruinsma, and P. Schaeffer (2013), Neural networks to predict exosphere temperature corrections, *Space Weather*, *11*, 592–602, doi:10.1002/2013SW000969.

Cook, G. E. (1965), Satellite drag coefficients, *Planet. Space Sci.*, *13*, 929–946.

Ejiri, M. (1978), Trajectory traces of charged particles in the magnetosphere, *J. Geophys. Res.*, *83*, 4798–4810.

Fedrizzi, M., T. J. Fuller-Rowell, and M. V. Codrescu (2012), Global Joule heating index derived from thermospheric density physics-bases modeling and observations, *Space Weather*, *10*, S03001, doi:10.1029/2011SW000724.

Frey, W. R. (2013), *Modeling the Thermosphere as a Driven-Dissipative Thermodynamic System,* Master's Thesis, pp. 135, Air Force Institute of Technology, Wright-Patterson Air Force Base, Ohio.

Fuller-Rowell, T. J., and S. C. Solomon (2010), Flares, coronal mass ejections, and atmospheric responses, in *Space Storms and Radiation: Causes and Effects*, edited by C. J. Schrijver and G. L. Siscoe, pp. 321–357, Cambridge Univ. Press, New York.

Jacchia, L. G. (1977), Thermospheric temperature, density, and composition: New models, *SAO Spec. Rep*, 375, 15 March.

Knipp, D. J., W. K. Tobiska, and B. A. Emery (2004), Direct and indirect thermospheric heating sources for solar cycles 21–23, *Sol. Phys.*, *224*, 495–505.

Knipp, D., L. Kilcommons, L. Hunt, M. Mlynczak, V. Pilipenko, B. Bowman, Y. Deng, and K. Drake (2013), Thermospheric damping response to sheath-induced geospace storms, *Geophys. Res. Lett.*, *40*, 1263–1267, doi:10.1002/grl.50197.

Lagarias, J. C., J. A. Reeds, M. H. Wright, and P. E. Wright (1998), Convergence properties of the Nelder Mead simplex method in low dimensions, *SIAM J. Optim.*, *9*, 112–147.

Liu, R., H. Lühr, E. Doornbos, and S. Y. Ma (2010), Thermospheric mass density variations during geomagnetic storms and a prediction model based on the merging electric field, *Ann. Geophys.*, *28*, 1633–1645, doi:10.5194/angeo-28-1633-2010.

Marcos, F. A., B. R. Bowman, and R. E. Sheehan (2006), Accuracy of Earth's thermospheric neutral density models, *AIAA Astrodynamics Specialist Conference, AIAA 2006-6167*, doi:10.2514/6.2006-6167.

Marcos, F. A., S. T. Lai, C. Y. Huang, C. S. Lin, J. M. Retterer, S. H. Delay, and E. Sutton (2010), Towards Next Level Satellite Drag Modeling, *AIAA Atmospheric and Space Environments Conference, AIAA2010-7840*, doi:10.2514/6.2010-7840.

Millward, G. H., I. C. F. Müller-Wodarg, A. D. Aylward, T. J. Fuller-Rowell, A. D. Richmond, and R. J. Moffett (2001), An investigation into the influence of tidal forcing on F region equatorial vertical ion drift using a global ionosphere-thermosphere model with coupled electrodynamics, *J. Geophys. Res.*, *106*, 24,733–24,744, doi:10.1029/2000JA000342.

Moe, K., and M. M. Moe (2011), Operational models and drag-derived density trends in the thermosphere, *Space Weather*, *9*, S00E10, doi:10.1029/2010SW000650.

Picone, J. M., A. E. Hedin, D. P. Drob, and A. C. Aikin (2002), NRLMSISE-00 empirical model of the atmosphere: Statistical comparisons and scientific issues, *J. Geophys. Res.*, *114*, A01312, doi:10.1029/2008JA013643.

Robinson, R. M., and R. R. Vondrak (1984), Measurements of the E Region Ionization and Conductivity Produced by Solar Illumination at High Latitudes, *J. Geophys. Res.*, *89*, 3951–3956.

Storz, M. F., B. R. Bowman, J. I. Branson, S. J. Casali, and W. K. Tobiska (2005), High accuracy satellite drag model (HASDM), *Adv. Space Res.*, *36*, 2497–2505, doi:10.1016/j.asr.2004.02.020.

Sutton, E. K. (2011), Accelerometer-Derived atmospheric densities from the CHAMP and GRACE satellites: Version 2.3, *AFRL Technical Memo*; DTIC # ADA537198.

Tapley, B. D., S. Bettadpur, M. Watkins, and C. Reigber (2004), The gravity recovery and climate experiment: Mission overview and early results, *Geophys. Res. Lett.*, *31*, L09607, doi:10.1029/2004GL019920.

Tobiska, W. K., T. Woods, F. Eparvier, R. Viereck, L. Floyd, D. Bouwer, G. Rottman, and O. R. White (2000), The SOLAR2000 empirical solar irradiance model and forecast tool, *J. Atmos. Sol. Terr. Phys.*, *62*, 1233–1250.

Weimer, D. R. (2005), Predicting surface geomagnetic variations using ionospheric electrodynamic models, *J. Geophys. Res.*, *110*, A12307, doi:10.1029/2005JA011270.

Weimer, D. R., B. R. Bowmann, E. K. Sutton, and W. K. Tobiska (2011), Predicting global average thermospheric temperature changes resulting from auroral heating, *J. Geophys. Res.*, *116*, A01312, doi:10.1029/2010JA015685.

Wilson, G. R., D. R. Weimer, J. O. Wise, and F. A. Marcos (2006), Response of the thermosphere to Joule heating and particle precipitation, *J. Geophys. Res.*, *111*, A10314, doi:10.1029/2005JA011274.

Wise, J. O., W. J. Burke, and E. K. Sutton (2012), Globally averaged exospheric temperatures derived from CHAMP and GRACE accelerometer measurements, *J. Geophys. Res.*, *117*, A04312, doi:10.1029/2011JA017108.

Wright, D. (2007), Space debris, *Phys. Today*, *60*, 35–40.